Electronic Supplementary Information

Bimetallic MOF-based catalysts with enhanced activity for electrochemical hydrogen evolution in acid and alkaline electrolytes

Rui-Zhe Zhang[a,b]*, Lele Lu[a], Peng Cheng[a] and Wei Shi[a]*

[a]Frontiers Science Center for New Organic Matter, Key Laboratory of Advanced Energy Materials Chemistry (MOE), State Key Laboratory of Advanced Chemical Power Sources, College of Chemistry, Nankai University, Tianjin 300071, China

[b]School of Chemistry and Pharmaceutical Engineering, Shandong First Medical University & Shandong Academy of Medical Sciences, Jinan 250000, China

Contents

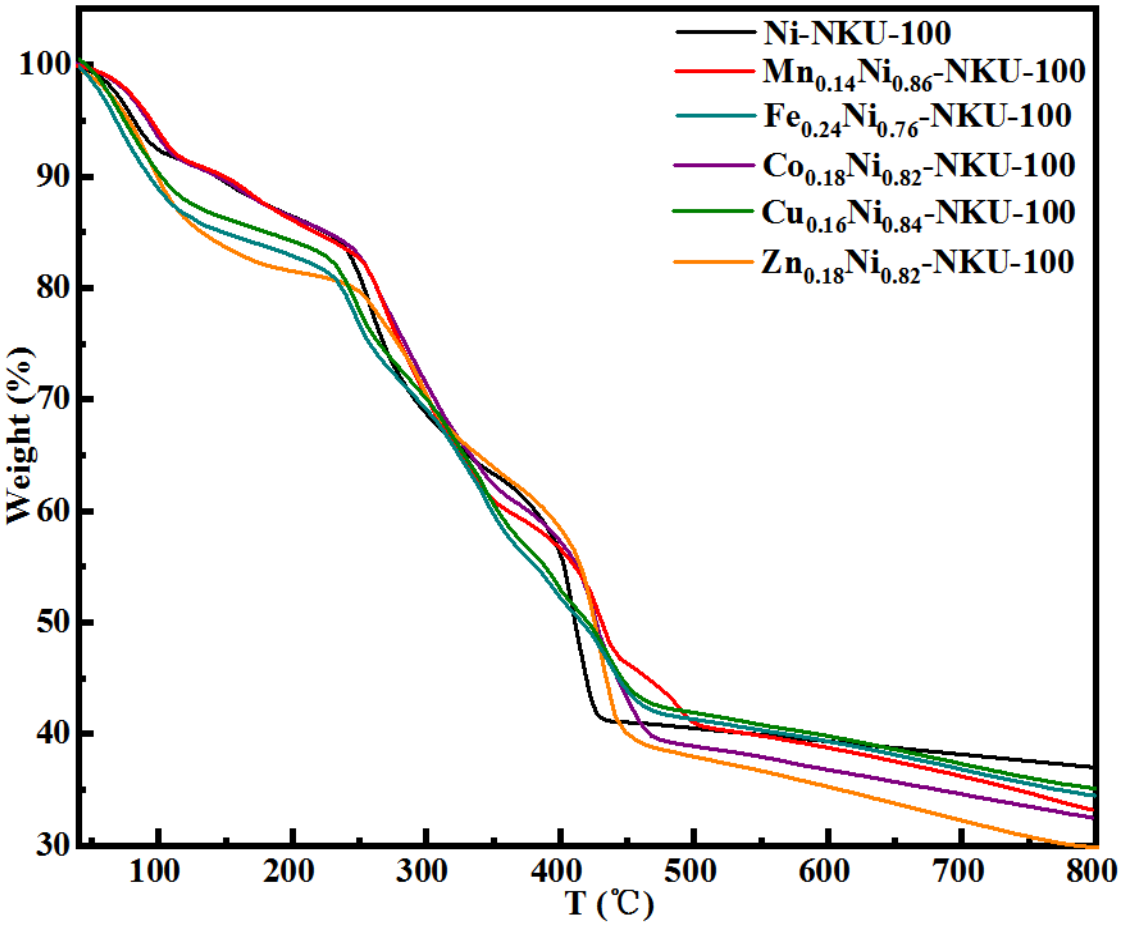

Fig. S1 Thermogravimetric analysis of Ni-NKU-100 and M_xNi_{1-x}-NKU-100 (M = Mn, Fe, Co, Cu, Zn).

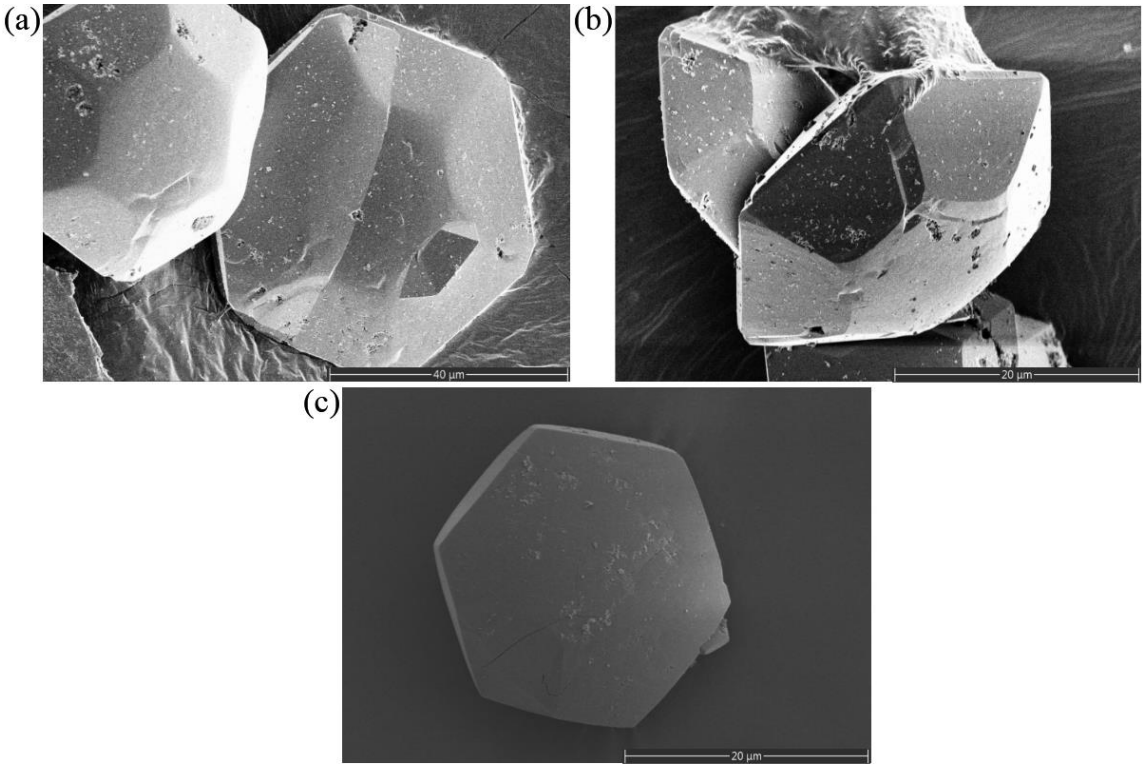

Fig. S2 FESEM images of Ni-NKU-100 (a), $Cu_{0.16}Ni_{0.84}$-NKU-100 (b) and $Fe_{0.24}Ni_{0.76}$-NKU-100 (c).

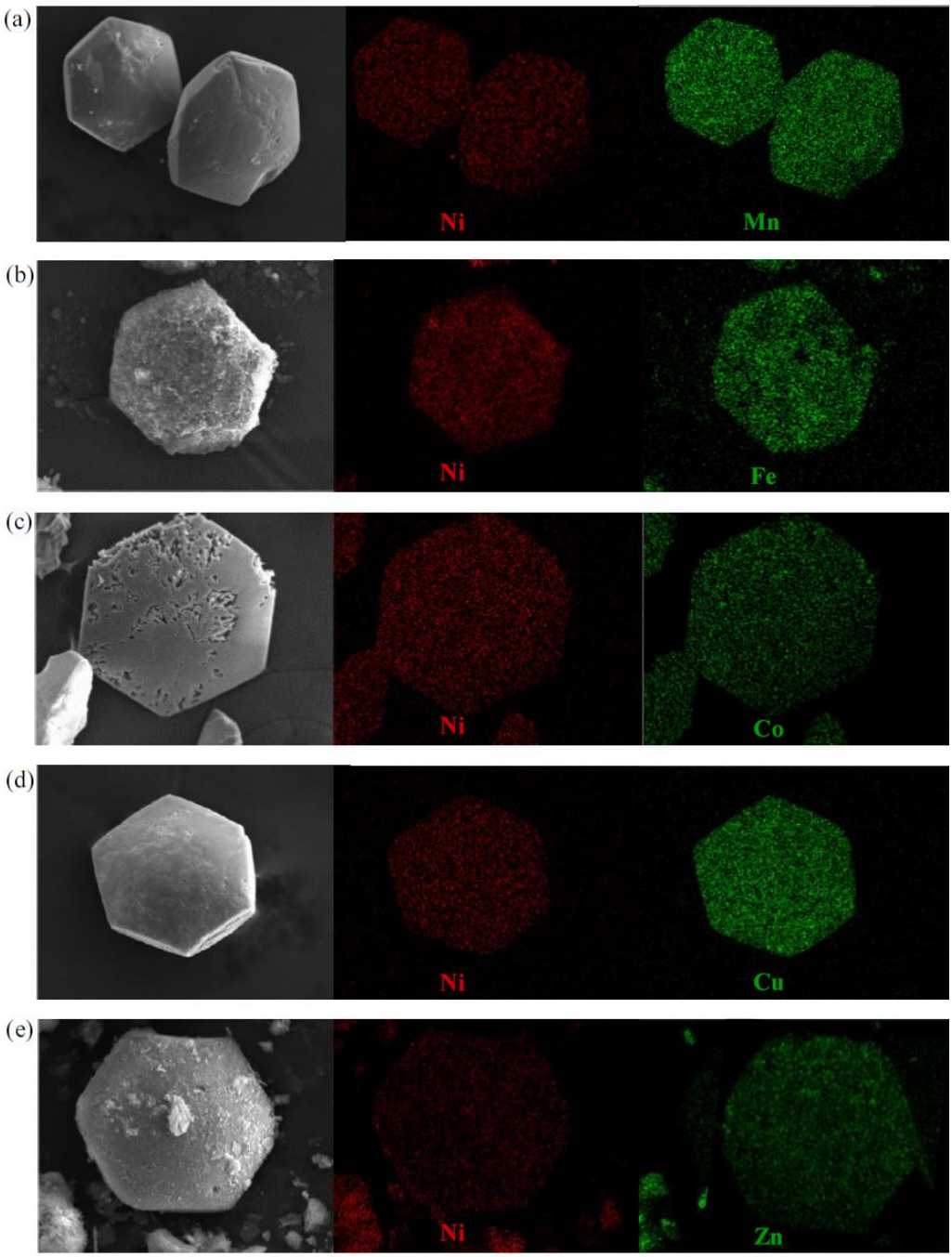

Fig. S3 SEM images and EDS elemental mappings of $Mn_{0.14}Ni_{0.86}$-NKU-100 (a), $Fe_{0.24}Ni_{0.76}$-NKU-100 (b), $Co_{0.18}Ni_{0.82}$-NKU-100 (c), $Cu_{0.16}Ni_{0.84}$-NKU-100 (d), and $Zn_{0.18}Ni_{0.82}$-NKU-100 (e).

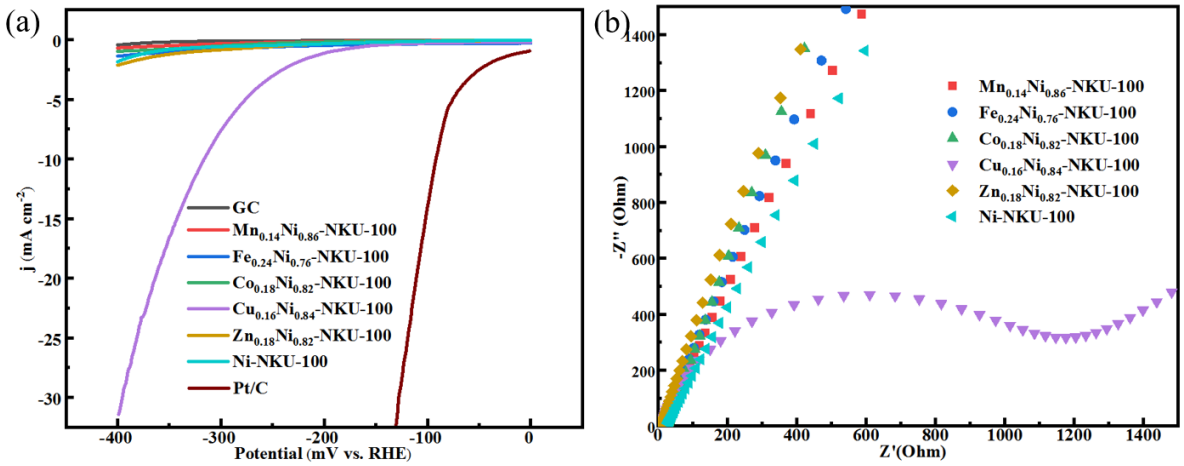

Fig. S4 (a) LSV curves at a scan rate of 5 mV·s^{-1} and (b) EIS Nyquist plots of M_xNi_{1-x}-NKU-100 (M = Mn, Fe, Co, Cu, Zn) in 0.5 M H_2SO_4 electrolyte.

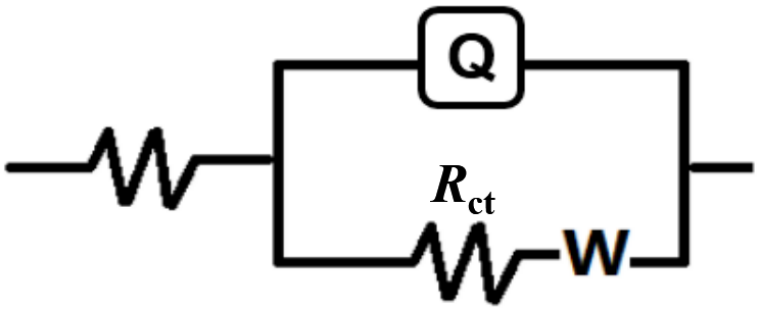

Fig. S5 The equivalent circuit for fitting electrochemical impedance.

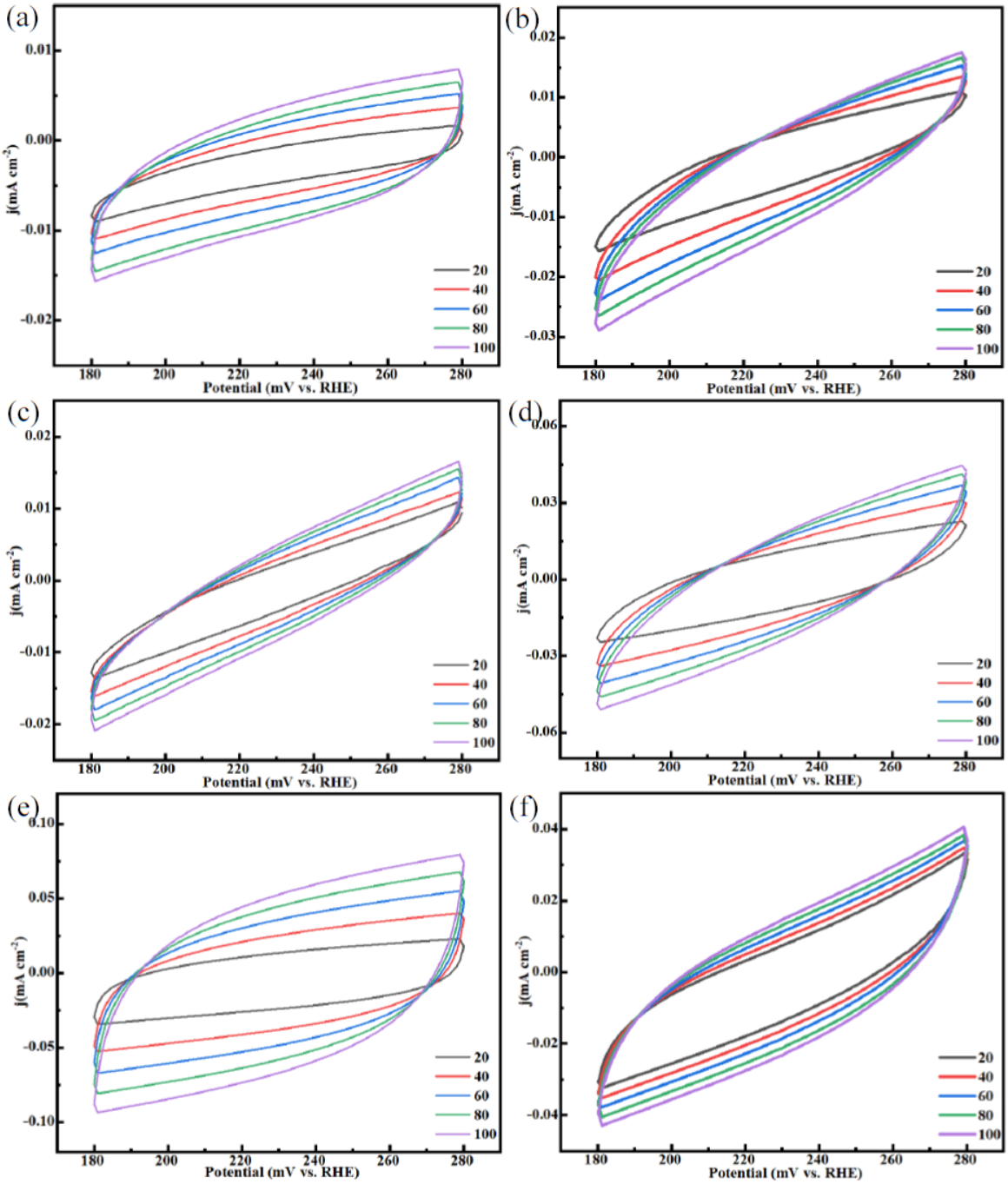

Fig. S6 CV curves of (a) Ni-NKU-100, (b) $Cu_{0.09}Ni_{0.91}$-NKU-100, (c) $Cu_{0.11}Ni_{0.89}$-NKU-100, (d) $Cu_{0.16}Ni_{0.84}$-NKU-100, (e) $Cu_{0.22}Ni_{0.78}$-NKU-100 and (f) $Cu_{0.25}Ni_{0.75}$-NKU-100 at the scan rate range from 20 to 100 mV s^{-1} in 0.5 M H_2SO_4 electrolyte.

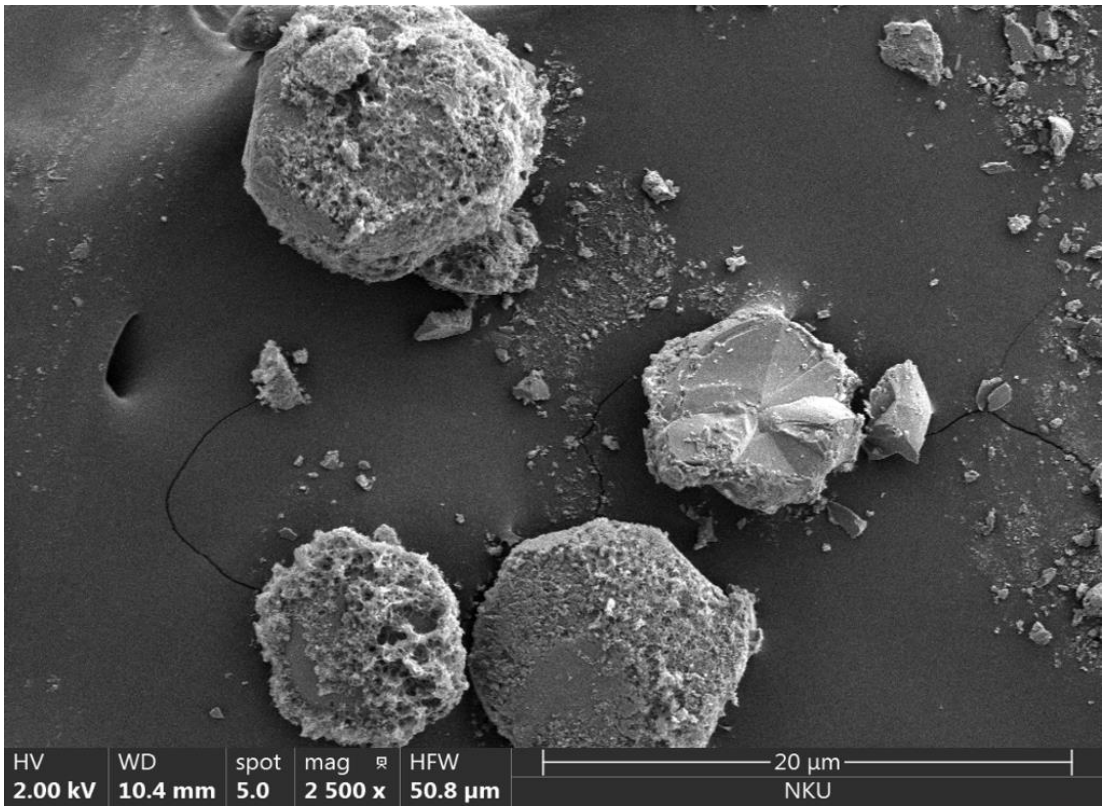

Fig. S7 SEM images of $Cu_{0.22}Ni_{0.78}$-NKU-100 after long-time electrocatalytic test in 0.5 M H_2SO_4 electrolyte.

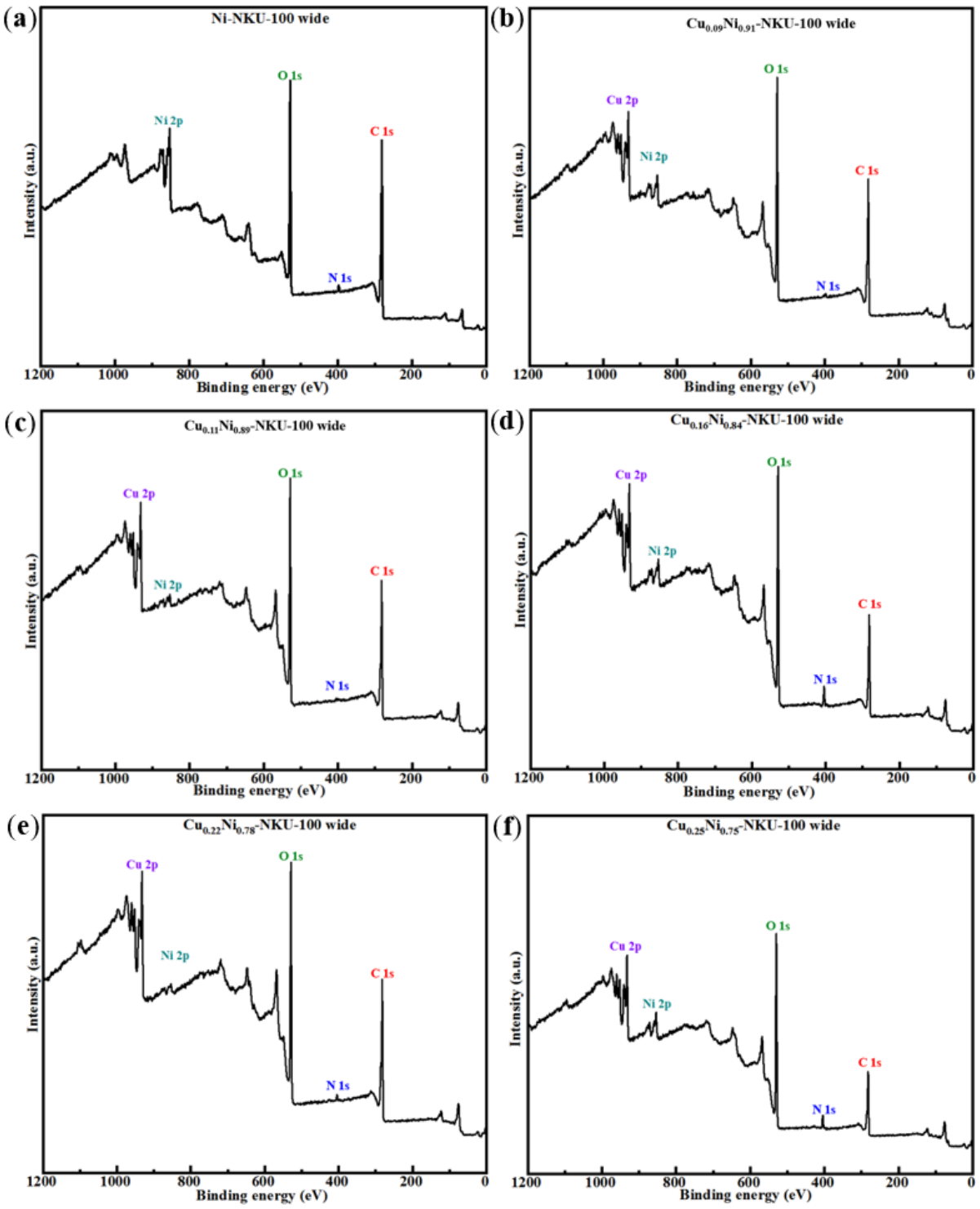

Fig. S8 XPS wide spectra of (a) Ni-NKU-100, (b) $Cu_{0.09}Ni_{0.91}$-NKU-100, (c) $Cu_{0.11}Ni_{0.89}$-NKU-100, (d) $Cu_{0.16}Ni_{0.84}$-NKU-100, (e) $Cu_{0.22}Ni_{0.78}$-NKU-100 and (f) $Cu_{0.25}Ni_{0.75}$-NKU-100.

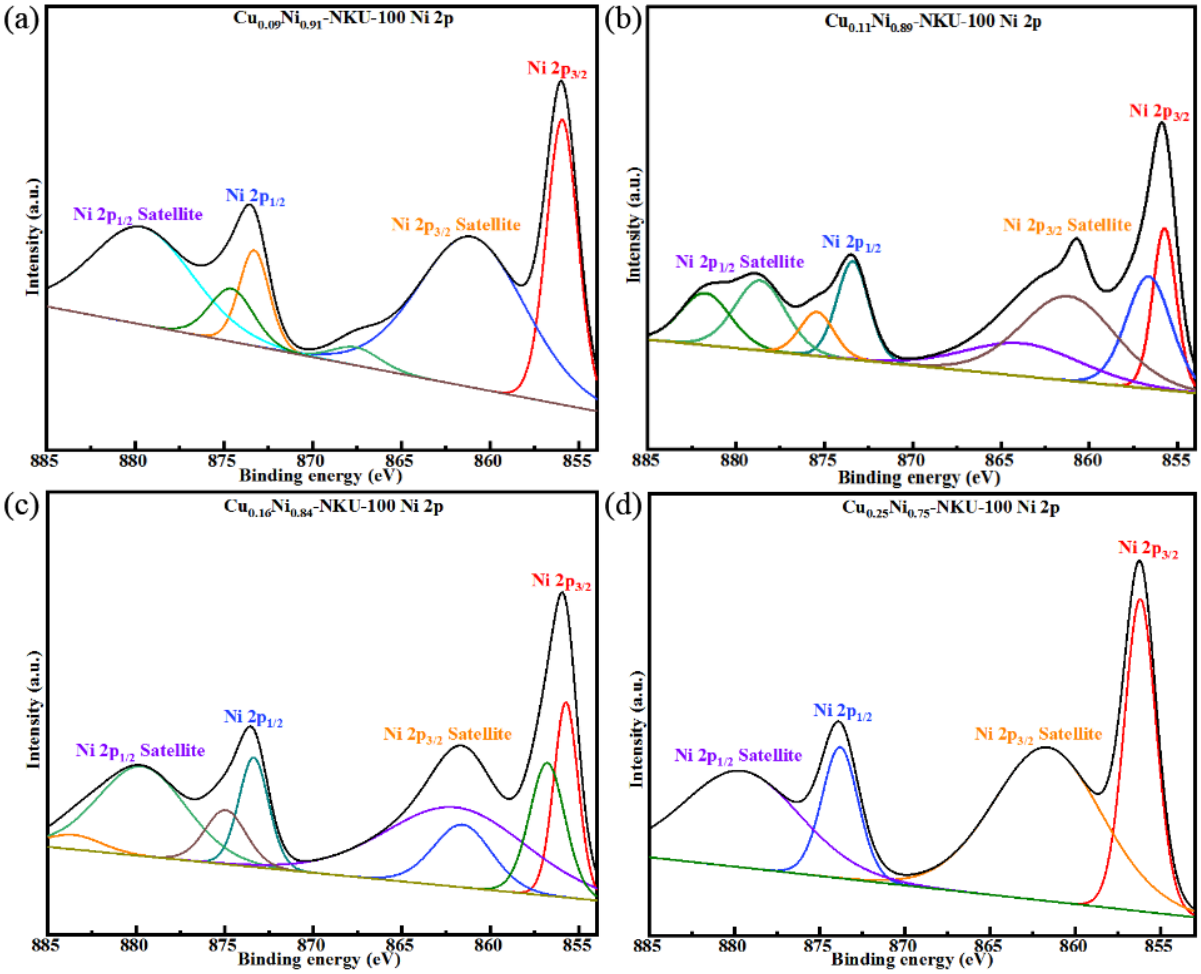

Fig. S9 High-resolution XPS of Ni 2p for (a) $Cu_{0.09}Ni_{0.91}$-NKU-100, (b) $Cu_{0.11}Ni_{0.89}$-NKU-100, (c) $Cu_{0.16}Ni_{0.84}$-NKU-100 and (d) $Cu_{0.25}Ni_{0.75}$-NKU-100.

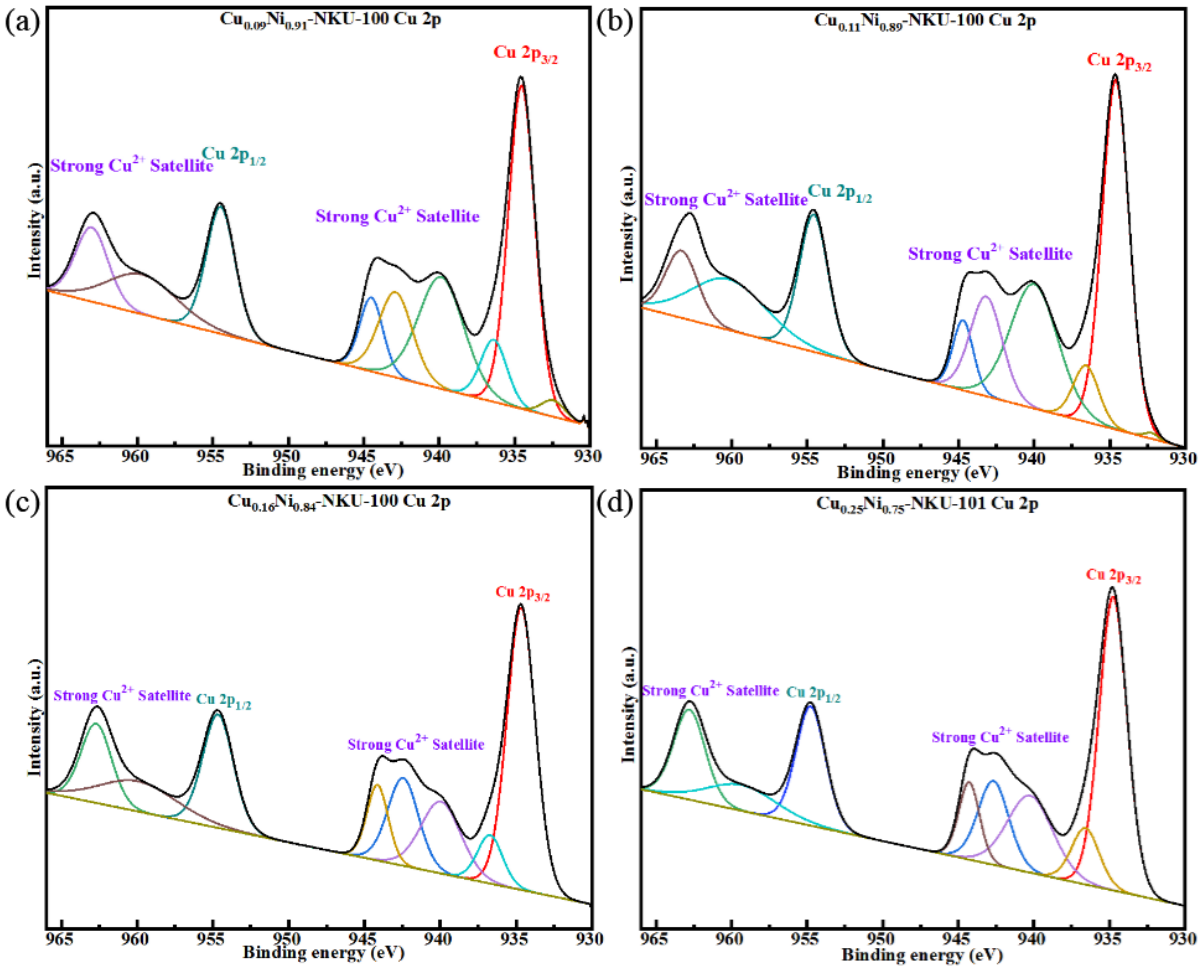

Fig. S10 High-resolution XPS of Cu 2p for (a) $Cu_{0.09}Ni_{0.91}$-NKU-100, (b) $Cu_{0.11}Ni_{0.89}$-NKU-100, (c) $Cu_{0.16}Ni_{0.84}$-NKU-100 and (d) $Cu_{0.25}Ni_{0.75}$-NKU-100.

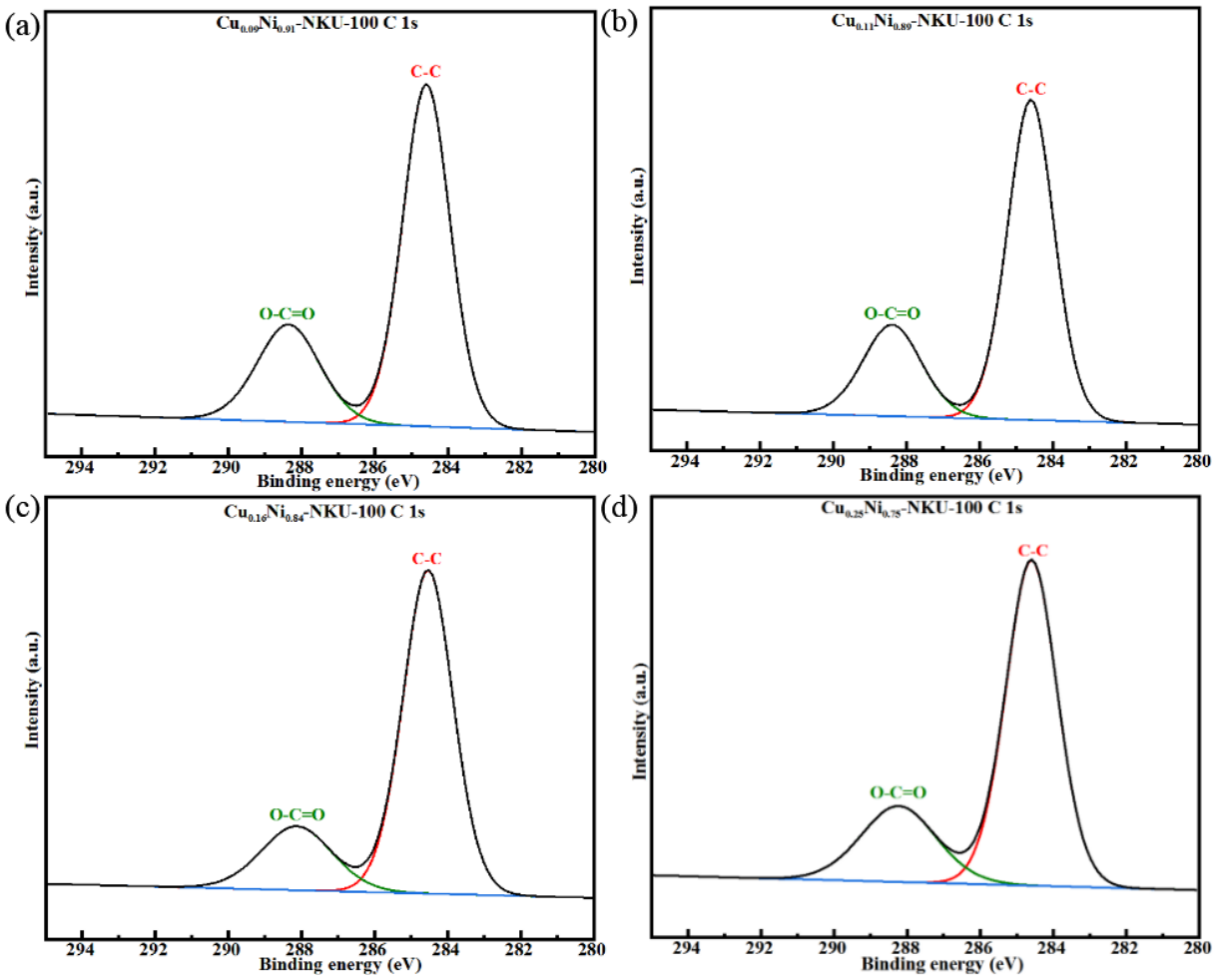

Fig. S11 High-resolution XPS of C 1s for (a) $Cu_{0.09}Ni_{0.91}$-NKU-100, (b) $Cu_{0.11}Ni_{0.89}$-NKU-100, (c) $Cu_{0.16}Ni_{0.84}$-NKU-100 and (d) $Cu_{0.25}Ni_{0.75}$-NKU-100.

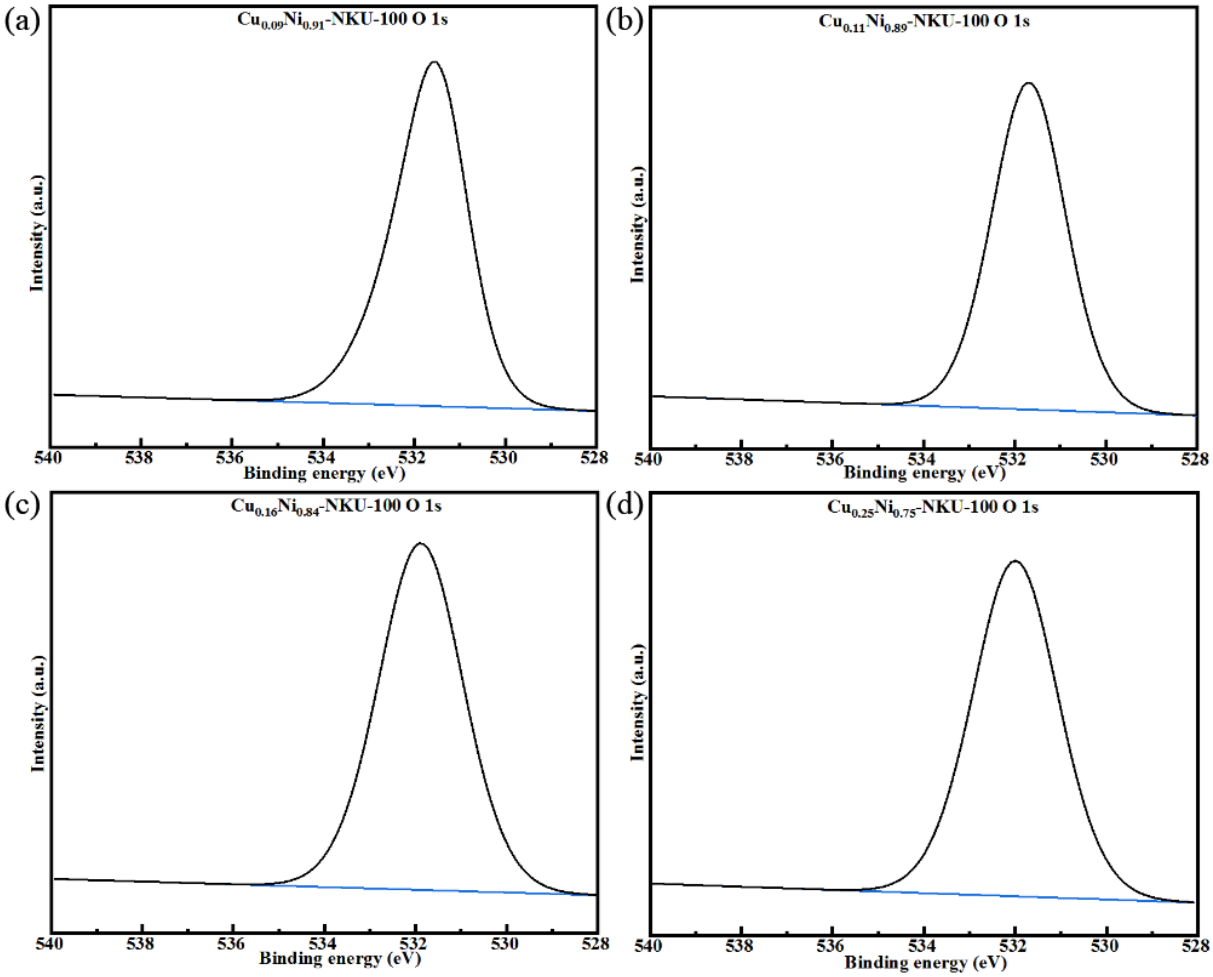

Fig. S12 High-resolution XPS of O 1s for (a) $Cu_{0.09}Ni_{0.91}$-NKU-100, (b) $Cu_{0.11}Ni_{0.89}$-NKU-100, (c) $Cu_{0.16}Ni_{0.84}$-NKU-100 and (d) $Cu_{0.25}Ni_{0.75}$-NKU-100.

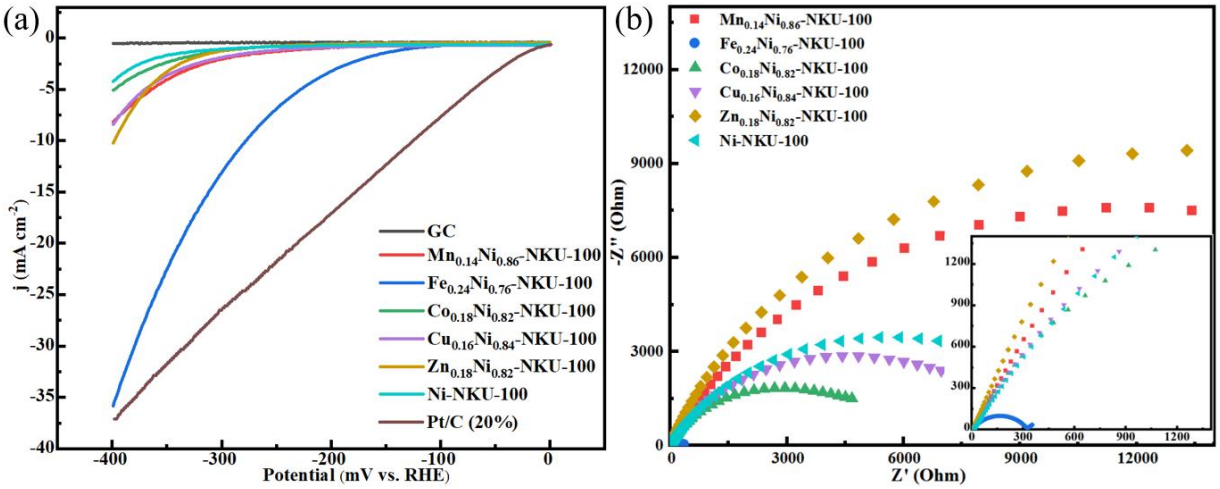

Fig. S13 (a) LSV curves at a scan rate of 5 mV·s^{-1} and (b) EIS Nyquist plots of M_xNi_{1-x}-NKU-100 (M = Mn, Fe, Co, Cu, Zn) in 1 M NaOH electrolyte.

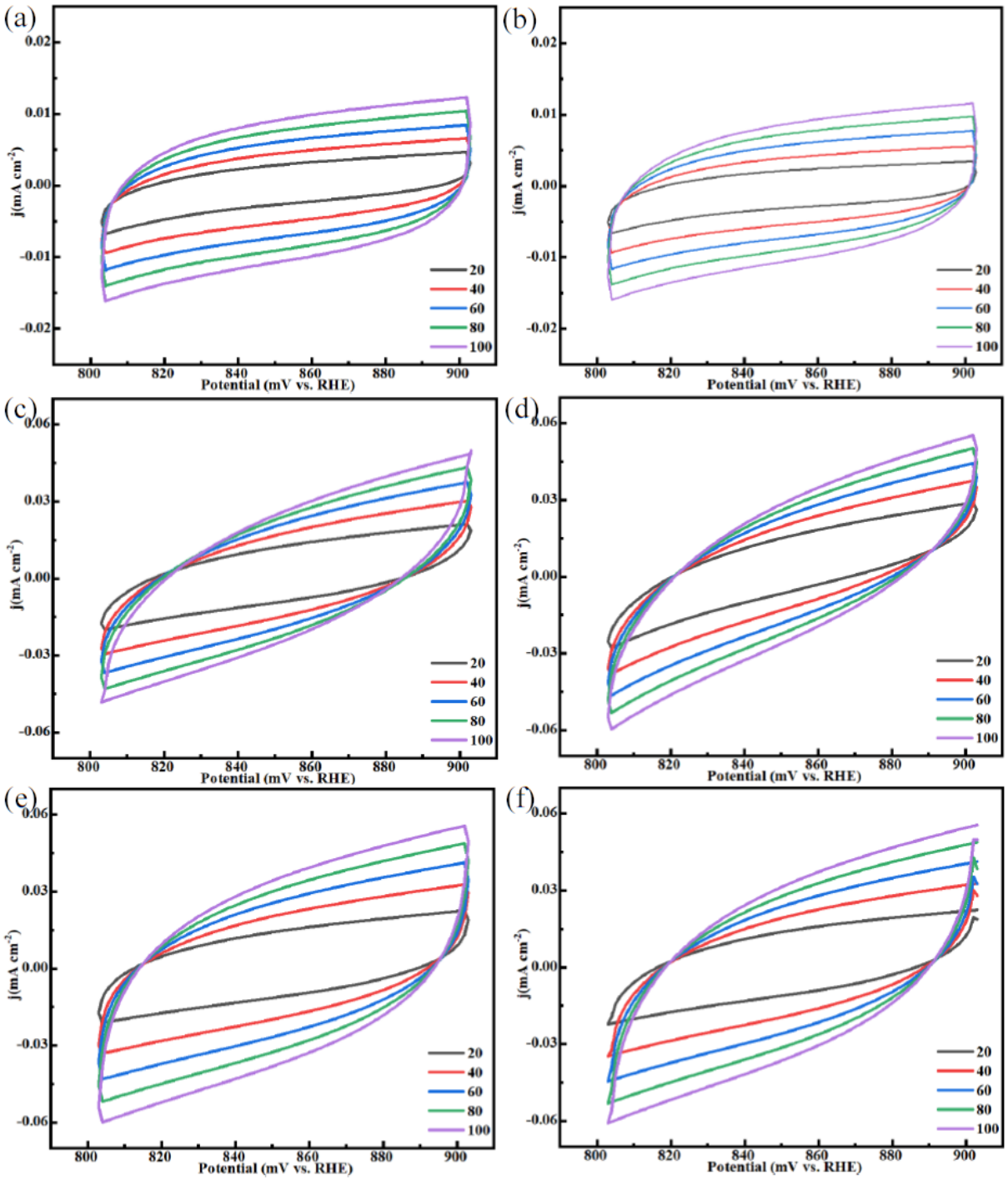

Fig. S14 CV curves of (a) Ni-NKU-100, (b) $Fe_{0.04}Ni_{0.96}$-NKU-100, (c) $Fe_{0.08}Ni_{0.92}$-NKU-100, (d) $Fe_{0.16}Ni_{0.84}$-NKU-100, (e) $Fe_{0.24}Ni_{0.76}$-NKU-100 and (f) $Fe_{0.34}Ni_{0.66}$-NKU-100 at the scan rate range from 20 to 100 mV s^{-1} in 1 M NaOH electrolyte.

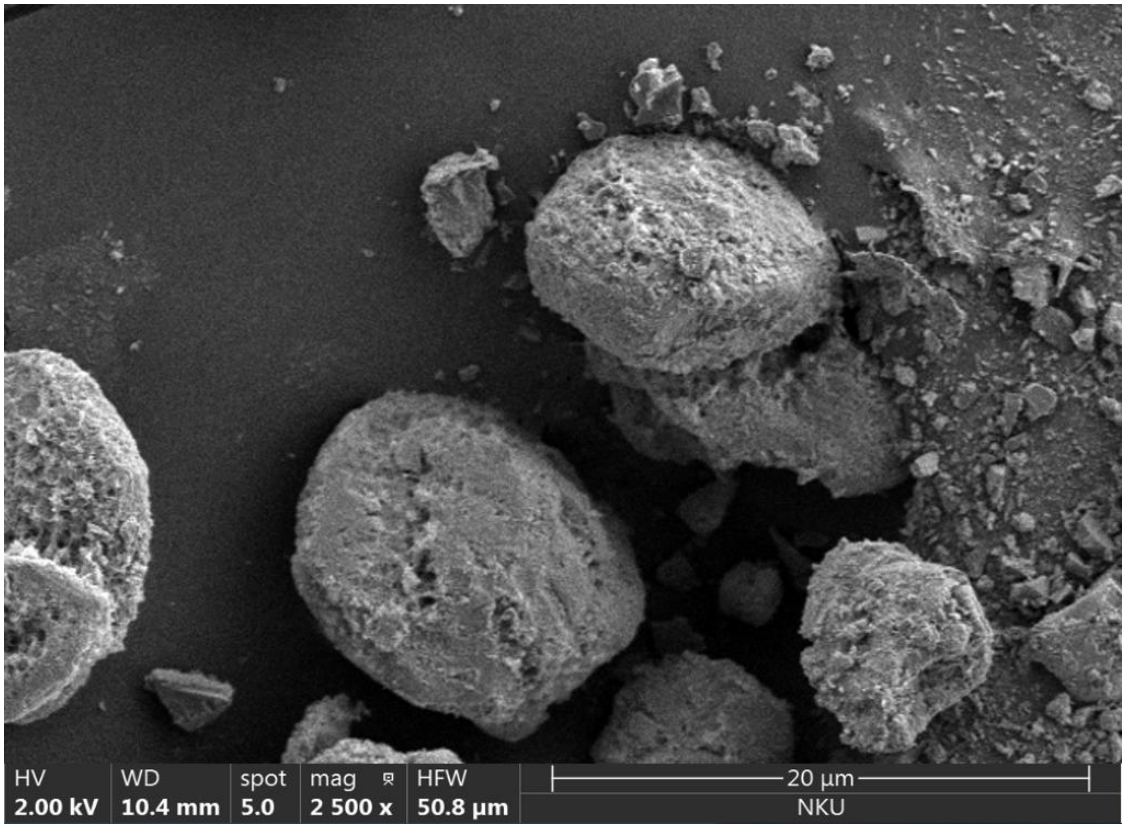

Fig. S15 SEM images of $Fe_{0.24}Ni_{0.76}$-NKU-100 after long-time electrocatalytic test in 1 M NaOH electrolyte.

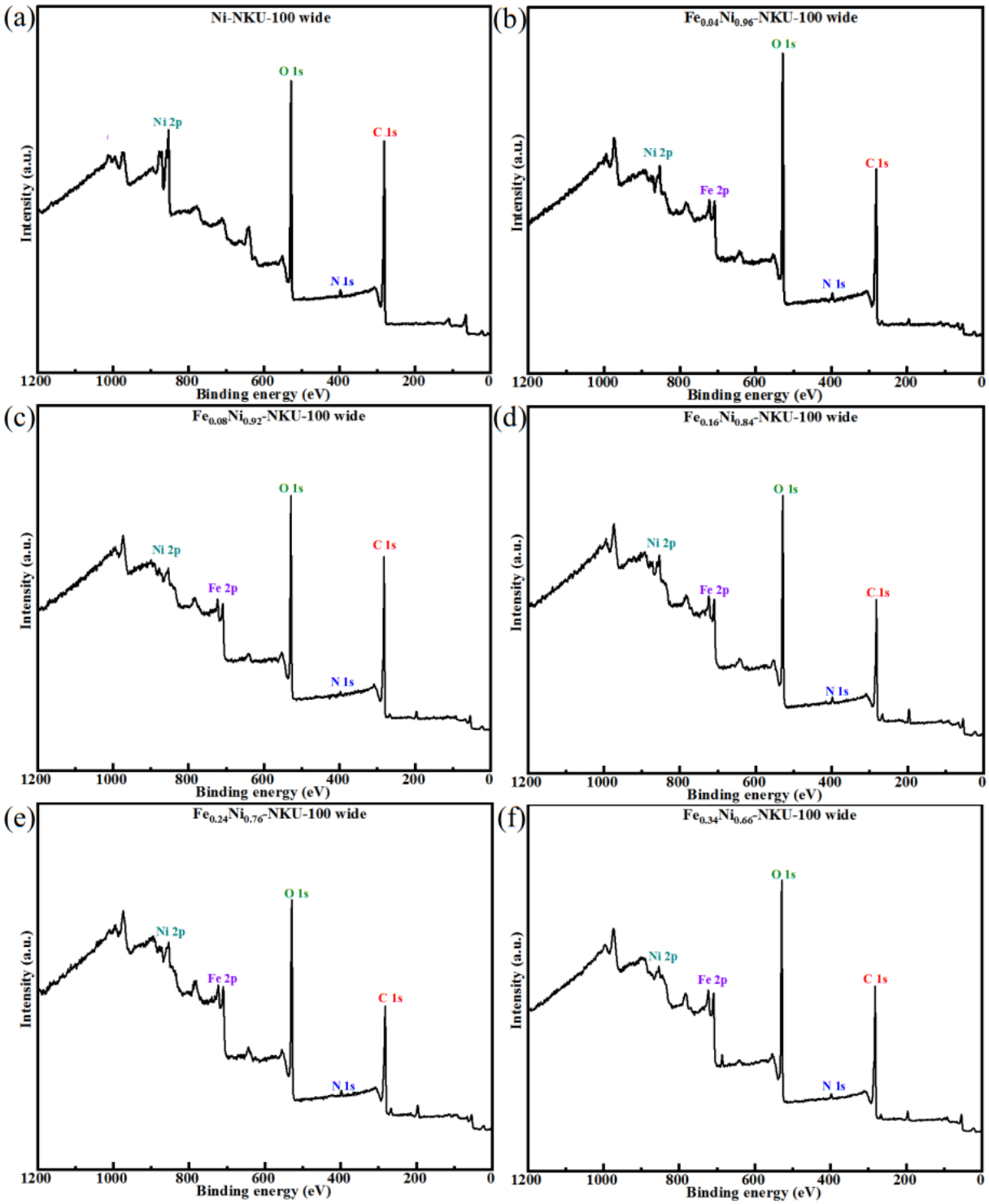

Fig. S16 XPS wide spectra of (a) Ni-NKU-100, (b) $Fe_{0.04}Ni_{0.96}$-NKU-100, (c) $Fe_{0.08}Ni_{0.92}$-NKU-100, (d) $Fe_{0.16}Ni_{0.84}$-NKU-100, (e) $Fe_{0.24}Ni_{0.76}$-NKU-100 and (f) $Fe_{0.34}Ni_{0.66}$-NKU-100.

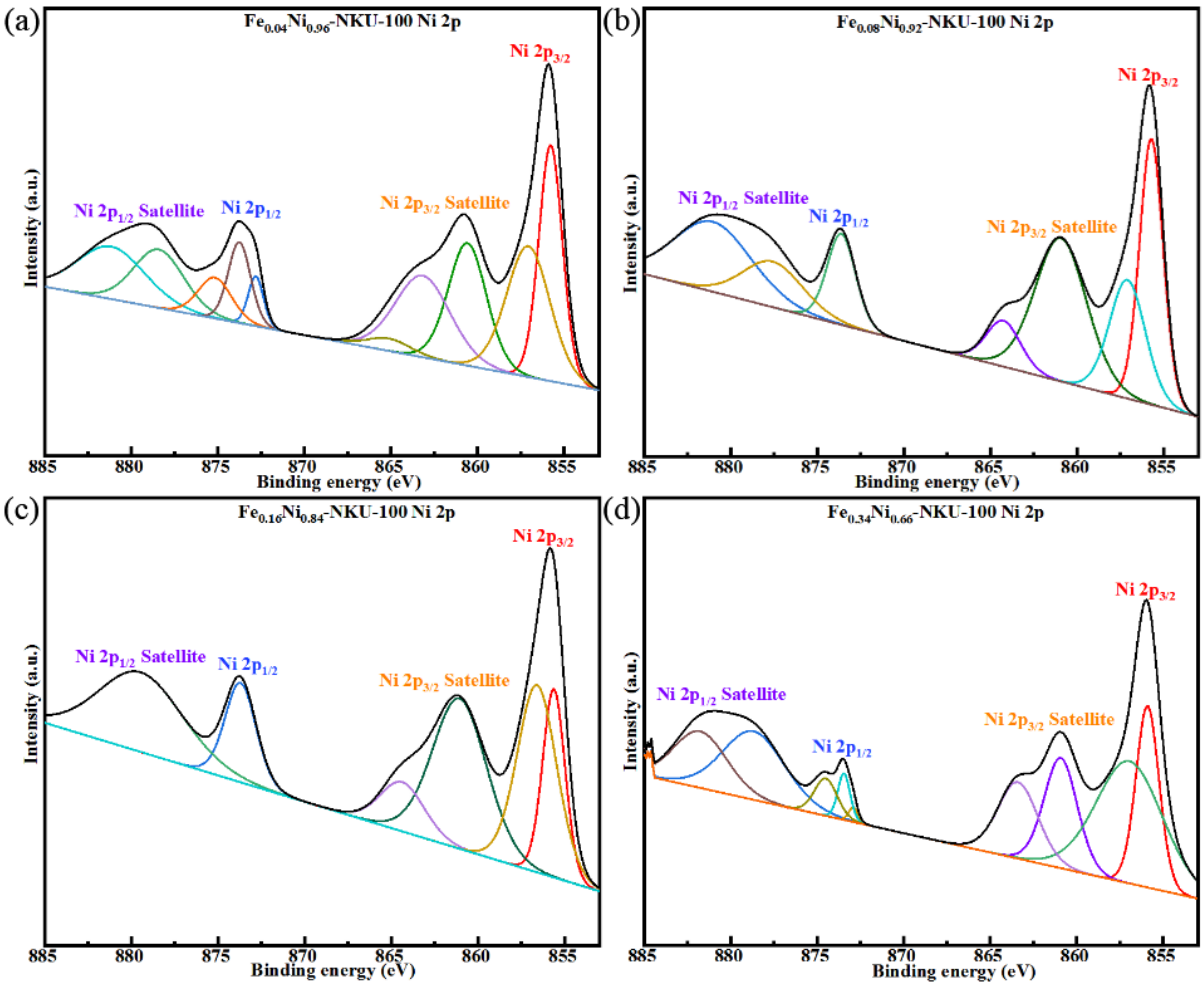

Fig. S17 High-resolution XPS of Ni 2p for (a) $Fe_{0.04}Ni_{0.96}$-NKU-100, (b) $Fe_{0.08}Ni_{0.92}$-NKU-100, (c) $Fe_{0.16}Ni_{0.84}$-NKU-100 and (d) $Fe_{0.34}Ni_{0.66}$-NKU-100.

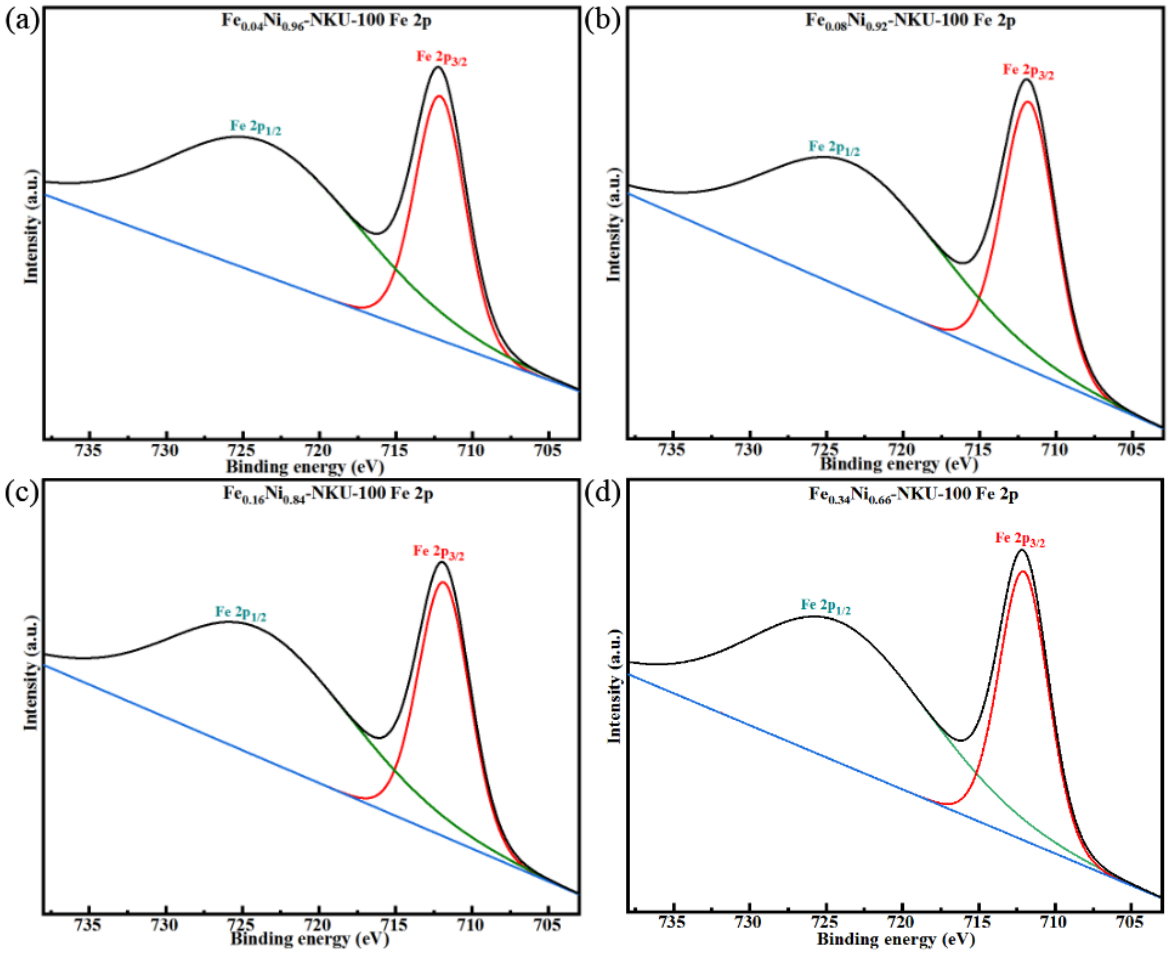

Fig. S18 High-resolution XPS of Fe 2p for (a) $Fe_{0.04}Ni_{0.96}$-NKU-100, (b) $Fe_{0.08}Ni_{0.92}$-NKU-100, (c) $Fe_{0.16}Ni_{0.84}$-NKU-100 and (d) $Fe_{0.34}Ni_{0.66}$-NKU-100.

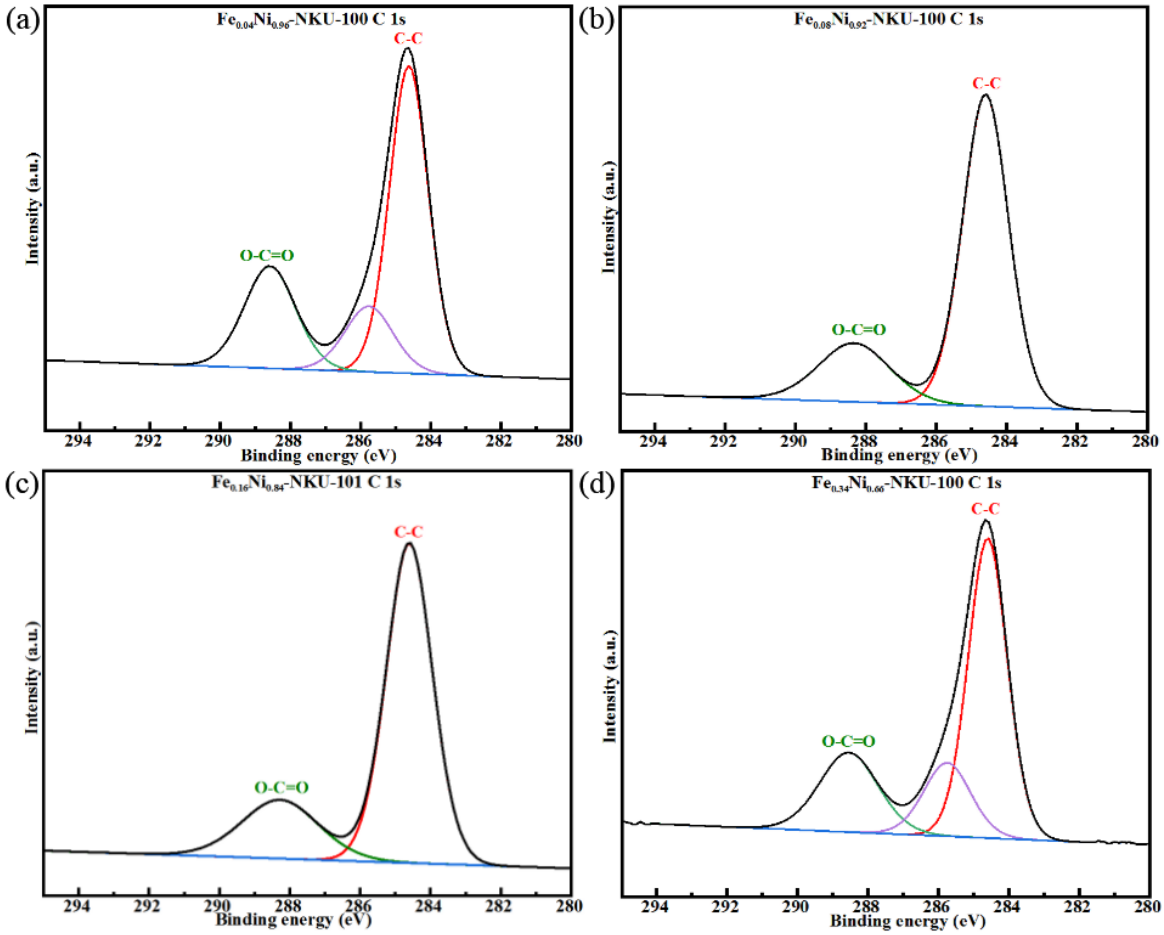

Fig. S19 High-resolution XPS of C 1s for (a) $Fe_{0.04}Ni_{0.96}$-NKU-100, (b) $Fe_{0.08}Ni_{0.92}$-NKU-100, (c) $Fe_{0.16}Ni_{0.84}$-NKU-100 and (d) $Fe_{0.34}Ni_{0.66}$-NKU-100.

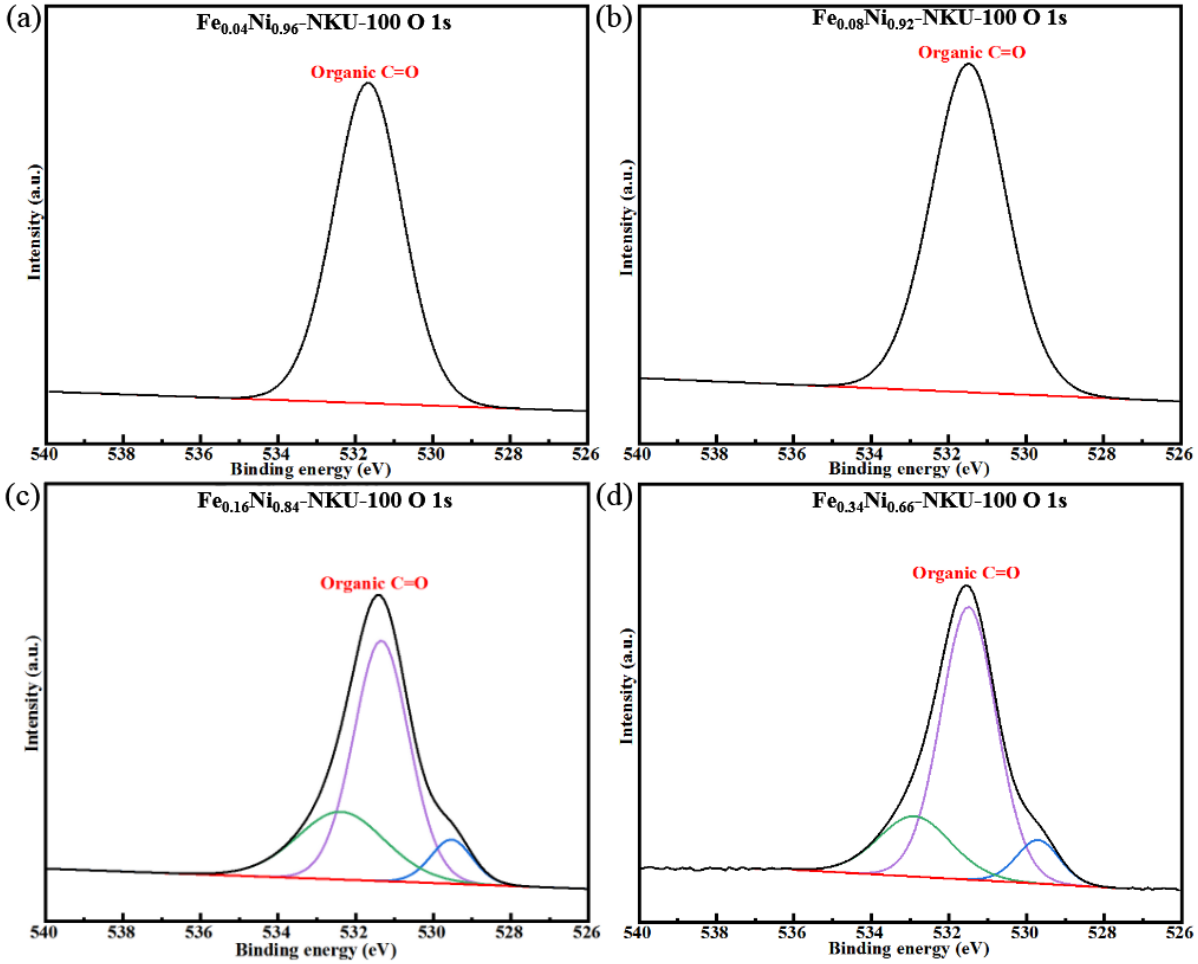

Fig. S20 High-resolution XPS of O 1s for (a) $Fe_{0.04}Ni_{0.96}$-NKU-100, (b) $Fe_{0.08}Ni_{0.92}$-NKU-100, (c) $Fe_{0.16}Ni_{0.84}$-NKU-100 and (d) $Fe_{0.34}Ni_{0.66}$-NKU-100.

Table S1 R_{ct} of Cu_xNi_{1-x}-NKU-100 in 0.5 M H_2SO_4 electrolyte.

Electrode material	R_{ct} (Ω)
Ni-NKU-100	86500
$Cu_{0.09}Ni_{0.91}$-NKU-100	53400
$Cu_{0.11}Ni_{0.89}$-NKU-100	3729
$Cu_{0.16}Ni_{0.84}$-NKU-100	2768
$Cu_{0.22}Ni_{0.78}$-NKU-100	702
$Cu_{0.25}Ni_{0.75}$-NKU-100	1066

Table S2. MOF-based HER electrocatalysts applied in acidic electrolyte.

Catalysts	Categories	η_{10} (mV)	Electrolyte	Stability	Reference
Ni-NKU-100	3D MOF	224	0.5 M H_2SO_4	24 h	This work
$Cu_{0.22}Ni_{0.78}$-NKU-100					
Co-MOF	3D MOF	357	0.5 M H_2SO_4	96 h	[1]
Co-MOF	3D MOF	223	0.5 M H_2SO_4	72 h	[2]
THAT-Co-single layer	2D MOF	283	0.5 M H_2SO_4	4 h	[3]
THTA-Co-powder		332			
THTA-Co-graphene		230			
CTGU-9	3D MOF	424	0.5 M H_2SO_4	21 h	[4]
AB: CTGU-9=3: 4		128			
UU-100(Co)	3D MOF	450	$NaClO_4$ (0.1 M)/ acetate (0.2 M) buffer at pH 4	~5 h	[5]
THT-Ni	2D MOF	333	0.5 M H_2SO_4		[6]
Cu-MOF	3D MOF	440	1 M H_2SO_4		[7]
NENU-5	3D MOF	585	0.5 M H_2SO_4		[8]
HKUST-1		691			
NENU-500		237			
NENU-501		392			
NENU-499		570			
ε(trim)4/3		515			
NU-1000	3D MOF	640	0.1 M HCl	2 h	[9]
NU-1000_Ni-S	3D MOF + sulfide	238			
bulk NiFe-MOF	3D MOF	196	0.5 M H_2SO_4	2 h	[10]
HKUST-1 ED		590			
HKUST-1 HT		660			
Ni-NKU-100	3D MOF	324	0.5 M H_2SO_4	24 h	[11]
$Cu_{0.19}Ni_{0.81}$-NKU-101					

Tab. S3 R_{ct} of Fe_xNi_{1-x}-NKU-100 in 1 M NaOH electrolyte.

Electrode material	R_{ct} (Ω)
Ni-NKU-100	35070
$Fe_{0.04}Ni_{0.96}$-NKU-100	2115
$Fe_{0.08}Ni_{0.92}$-NKU-100	577
$Fe_{0.16}Ni_{0.84}$-NKU-100	410
$Fe_{0.24}Ni_{0.76}$-NKU-100	204
$Fe_{0.34}Ni_{0.66}$-NKU-100	809

Table S4. MOF-based HER electrocatalysts applied in alkaline electrolyte.

Catalysts	Categories	η_{10} (mV)	Electrolyte	Stability	Reference
Ni-NKU-100	3D MOF		1 M KOH		This work
$Fe_{0.24}Ni_{0.76}$-NKU-100		249		24 h	
Co-BDC	2D MOF	529	1 M KOH		[12]
Co-BDC-MoS_2	2D MOF + sulfide	248		15 h	
NiFe-MOF		134		5.5 h	
Ni-MOF	3D MOF	177	0.1 M KOH		[13]
bulk NiFe-MOF		196			
Co–BTC/CC	3D MOF	437	1 M KOH		[14]
CuCo-CAT	3D MOF	52	1 M KOH	10 h	[15]
$Fe(OH)_x$@Cu-MOF	3D MOF	112	1 M KOH	30 h	[16]
Fe_2Zn-MOF	3D MOF	221	0.1 M KOH	24 h	[17]
$Ni_3(Ni_3{\cdot}HAHATN)_2$	3D MOF	115	0.1 M KOH	10 h	[18]

References

1 X. Wang, J.Y. Luo, J.W. Tian, D.D. Huang, Y.P. Wu, S. Li and D.S. Li, Two new 3D isostructural Co/Ni-MOFs showing four-fold polyrotaxane-like networks: Synthesis, crystal structures and hydrogen evolution reaction, *Inorg. Chem. Comm.*, 2018, **98**, 141–144.

2 Y.C. Zhou, W.W. Dong, M.Y. Jiang, Y.P. Wu, D.S. Li, Z.F. Tian and J. Zhao, A new 3D 8-fold interpenetrating 66-dia topological Co-MOF: Syntheses, crystal structure, magnetic properties and electrocatalytic hydrogen evolution reaction, *J. Solid. State. Chem.*, 2019, **279**, 120929.

3 R. Dong, Z. Zheng, D.C. Tranca, J. Zhang, N. Chandrasekhar, S. Liu, X. Zhuang, G. Seifert and X. Feng, Immobilizing Molecular Metal Dithiolene-Diamine Complexes on 2D Metal-Organic Frameworks for Electrocatalytic H_2 Production, *Chem. Eur. J.*, 2017, **23**, 2255–2260.

4 W. Zhou, Y.P. Wu, X. Wang, J. Wu Tian, D.D. Huang, J. Zhao, Y.Q. Lan and D.S. Li, Improved conductivity of a new Co(II)-MOF by assembled acetylene black for efficient hydrogen evolution reaction, *CrystEngComm*, 2018, **20**, 4804–4809.

5 S. Roy, Z. Huang, A. Bhunia, A. Castner, A.K. Gupta, X. Zou and S. Ott, Electrocatalytic Hydrogen Evolution from a Cobaloxime-Based Metal-Organic Framework Thin Film, *J. Am. Chem. Soc.*, 2019, **141**, 15942–15950.

6 R. Dong, M. Pfeffermann, H. Liang, Z. Zheng, X. Zhu, J. Zhang and X. Feng, Large-area, Free-Standing, Two-Dimensional Supramolecular Polymer Single-Layer Sheets for Highly Efficient Electrocatalytic Hydrogen Evolution, *Angew. Chem. Int. Ed.*, 2015, **54**, 12058–12063.

7 D.H. He, J.J. Liu, Y. Wang, F. Li, B. Li and J.B. He, Electrocatalysis of the first electron transfer in hydrogen evolution reaction with an atomically precise Cu^{II}-organic framework catalyst, *Electrochim. Acta.*, 2019, **308**, 285–294.

8 J.S. Qin, D.Y. Du, W. Guan, X.J. Bo, Y.F. Li, L.P. Guo, Z.M. Su, Y.Y. Wang, Y.Q. Lan and H.C. Zhou, Ultrastable Polymolybdate-Based Metal-Organic Frameworks as Highly Active Electrocatalysts for Hydrogen Generation from Water, *J. Am. Chem. Soc.*, 2015, **137**, 7169–7177.

9 I. Hod, P. Deria, W. Bury, J.E. Mondloch, C.W. Kung, M. So, M.D. Sampson, A.W. Peters, C.P. Kubiak, O. K. Farha and J. T. Hupp, A porous proton-relaying metal-organic framework material that accelerates electrochemical hydrogen evolution, *Nat. Commun.*, 2015, **6**, 8304.

10 X.F. Li, M.Y. Lu, H.Y. Yu, T.H. Zhang, J. Liu, J.H. Tian and R. Yang, Copper-Metal Organic Frameworks Electrodeposited on Carbon Paper as an Enhanced Cathode for the Hydrogen Evolution Reaction, *ChemElectroChem.*, 2019, **6**, 4507–4510.

11 R.-Z. Zhang, L.-L. Lu, Z.-H. Chen, X. Zhang, B.-Y. Wu, W. Shi and P. Cheng, Bimetallic Cage-Based Metal-Organic Frameworks for Electrochemical Hydrogen Evolution Reaction with Enhanced Activity, *Chem. Eur. J.*, 2022, **28**, **28**, e202200401.

12 D. Zhu, J. Liu, Y. Zhao, Y. Zheng and S.Z. Qiao, Engineering 2D Metal–Organic Framework/MoS_2 Interface for Enhanced Alkaline Hydrogen Evolution, *Small*, 2019, **15**, 1805511.

13 J. Duan, S. Chen and C. Zhao, Ultrathin metal-organic framework array for efficient electrocatalytic water splitting, *Nat. Commun.*, 2017, **8**, 15341.

14 S.N. Shreyanka, J. Theerthagiri, S.J. Lee, Y. Yu and M.Y. Choi, Multiscale design of 3D metal–organic frameworks (M−BTC, M: Cu, Co, Ni) via PLAL enabling bifunctional electrocatalysts for robust overall water splitting, *Chem. Eng. J.*, 2022, **446**, 137045.

15 B. Geng, F. Yan, X. Zhang, Y. He, C. Zhu, S.-L. Chou, X. Zhang and Y. Chen, Conductive CuCo-Based Bimetal Organic Framework for Efficient Hydrogen Evolution, *Adv. Mater.*, 2021, **33**, 2106781.

16 W. Cheng, H. Zhang, D. Luan and X.W. (David) Lou, Exposing unsaturated Cu_1-O_2 sites in nanoscale Cu-MOF for efficient electrocatalytic hydrogen evolution, *Sci. Adv.*, 2021, **7**, eabg2580.

17 M. Gu, S.-C. Wang, C. Chen, D. Xiong and F.-Y. Yi, Iron-Based Metal–Organic Framework System as an Efficient Bifunctional Electrocatalyst for Oxygen Evolution and Hydrogen Evolution Reactions, *Inorg. Chem.*, 2020, **59**, **9**, 6078–6086.

18 H. Huang, Y. Zhao, Y. Bai, F. Li, Y. Zhang and Y. Chen, Conductive Metal–Organic Frameworks with Extra Metallic Sites as an Efficient Electrocatalyst for the Hydrogen Evolution Reaction, *Adv. Sci.*, 2020, **7**, 2000012.